


Perturbative computation of nonlinear harvesting through a path integral approach

Martín E. Giuliano , Bruno Combi , Matías G. dell’Erba , and Alejandro D. Sánchez 
 IFIMAR-CONICET Universidad Nacional de Mar del Plata, 7600 Mar del Plata, Argentina

 (Received 13 February 2023; accepted 10 December 2023; published 8 January 2024)

Statistical field theories provide powerful tools to study complex dynamical systems. In this work those tools are used to analyze the dynamics of a kinetic energy harvester, which is modeled by a system of coupled stochastic nonlinear differential equations and driven by colored noise. Using the Martin-Siggia-Rose response fields we analytically approach the problem through path integrals in the phase space and represent the moments that correspond to physical observables through Feynman diagrams. This analysis method is tested by comparing the solution to the linear case with previous analytical results. Through a perturbative expansion it is calculated how the nonlinearity affects, to the first order, the energy harvest supporting the results through numerical simulations.

DOI: [10.1103/PhysRevE.109.014210](https://doi.org/10.1103/PhysRevE.109.014210)

I. INTRODUCTION

The inevitable depletion of fossil fuels and the environmental pollution generated by their use present the need for a global energy transition towards renewable and clean energy sources. This must occur at all energy scales and in a multitude of different scenarios. An interesting application corresponds to environmental energy sources and their implementation in wireless systems to operate small devices such as sensors, actuators, and information engines [1–5]. These spatially distributed wireless nodes detect and communicate local information such as acceleration, temperature, pressure, air pollution, biological parameters, magnetic field, light intensity, etc.

The study of converting energy present in the environment into electrical energy is known as energy harvesting [1,4,6,7]. Several renewable energies in the environment are the wind, solar radiation, temperature or concentration gradients, kinetic energy in the form of mechanical vibrations, etc. In all of them the external force responsible for the movement can be considered deterministic as well as stochastic. The most outstanding types of systems for their power density, versatility and abundance, are the mechanical vibration energy harvesters that convert kinetic energy through electromagnetic, electrostatic, or piezoelectric transducers into electrical energy [1,8–10]. This conversion produces a loss of kinetic energy, which can be considered as an electrically induced damping.

Most vibration power generators are resonant systems that obtain maximum power when the resonance frequency of the generator matches the ambient vibration frequency. In its simplest version, the mass of the system is subject to Hooke’s law and therefore the mechanical force is linear. The system then harvests maximum energy from the ambient vibrations if the excitation frequency matches the natural frequency of the system, which is known as resonant energy harvesting. Outside the resonance bandwidth the response of the system and, therefore, the power obtained drop drastically. Adaptive kinetic energy harvesters are developed to increase their operating frequency range, thus addressing the bandwidth

limitation [11]. Among the possible strategies of adaptive harvesters is the application of nonlinear oscillators, which have been shown to be an important ingredient to improve the yield of the harvester of kinetic energy [12–18].

A general model for the conversion of kinetic energy from a vibrating mass into electrical energy can be formulated without the need to specify the mechanism by which the transduction takes place. The model is not a specific device and therefore the conversion mechanism does not need to be set [19]. In this work we analytically study, by means of a perturbative expansion, the effect of nonlinearity on the Duffing potential to improve the harvested power, the efficiency of the system, and the effective bandwidth. The results obtained are contrasted with the numerical solution of the equations.

In Sec. II, we present the model and the formal solution using path integrals. In Sec. III, we solve the linear case exactly by comparing the results with those presented in [20] and we introduce the Feynman diagrams which we use to pictorially represent the calculated moments. In Sec. IV, by means of a perturbative expansion and with the help of the Feynman diagrams introduced in the previous section, we analytically calculate the first-order nonlinear case, numerically corroborating the results. Finally in Sec. V we give our conclusions.

II. MODEL

The harvester model we study (based on the general model [1]) consists of a one-dimensional Duffing’s oscillator—i.e., an oscillating mass, m , in a potential $U(x_I) = \alpha x_I^2/2 + \beta x_I^4/24$ —coupled to a transducer system (either piezoelectric, electrostatic, or electromagnetic)¹ that transforms mechanical energy into electrical inducing an electrical voltage V_I . Then, the voltage is connected to a load resistance R . The stochastic differential equations for a kinetic energy harvester arise from

¹Other transducer systems use different variables and parameters but the general structure of the equations is the same, allowing us to analyze the general issues.

applying Newton's second law to the mass m in addition to the constitutive relations of the transducer system,²

$$m \frac{d^2 x_I(s)}{ds^2} = -\gamma_m \frac{dx_I(s)}{ds} - k_V V_I(s) - \alpha x_I(s) - \frac{\beta}{6} x_I(s)^3 + \eta_I(s), \quad (1)$$

$$\frac{dV_I(s)}{ds} = k_c \frac{dx_I(s)}{ds} - \gamma_e V_I(s). \quad (2)$$

The variables x_I and V_I are the displacement of the oscillator and the electrical voltage induced in the transducer, respectively. The coefficient γ_m accounts for the damping of the mechanical oscillations, k_V and k_c are the couplings between the oscillation and the induced voltage, while $\gamma_e^{-1} = RC$ is the time constant of the circuit (given by the capacitance C of the system and the load resistance R). The system is driven by an external force, modeled with an Orstein-Uhlenbeck noise $\eta_I(s)$ with $\langle \eta_I(s) \rangle = 0$ and correlation $\langle \eta_I(s) \eta_I(s') \rangle = D e^{-\lambda_I |s-s'|}$.

Changing the variables to

$$s \rightarrow t = \frac{\gamma_m}{m} s, \quad (3)$$

$$x_I \rightarrow x = \frac{\gamma_m^2}{m\sqrt{D}} x_I, \quad (4)$$

$$V_I \rightarrow V = \frac{\gamma_m^2}{m\sqrt{D}k_c} V_I, \quad (5)$$

and renaming $k = mk_c k_V / \gamma_m^2$, $a = m\alpha / \gamma_m^2$, $b = m^3 D \beta / \gamma_m^6$, $\zeta = m\gamma_e / \gamma_m$, and $\lambda = m\lambda_I / \gamma_m$, we reduce the number of parameters. This choice of adimensionalization is arbitrary and the physical results do not depend on it. The values chosen for the parameters in the images are generic, as in Mendez *et al.* Using $\dot{x} = v$ (the dot indicates the t derivative) the equation of the system with the new dimensionless variables is

$$\dot{\mathbf{r}} = \mathbf{f}(\mathbf{r}) + \Xi(t), \quad (6)$$

where

$$\begin{aligned} \mathbf{r} &= (x, v, V, \eta)^T, \\ \mathbf{f}(\mathbf{r}) &= \left(v, -v - kV - ax - \frac{b}{6}x^3 + \eta, v - \zeta V, -\lambda\eta \right)^T, \\ \Xi &= (0, 0, 0, \sqrt{2\lambda}\xi)^T. \end{aligned} \quad (7)$$

Here the superscript T indicates transposed. As usual, we use a Gaussian white noise ξ —with $\langle \xi(t) \rangle = 0$ and $\langle \xi(t)\xi(t') \rangle = \delta(t-t')$ —to generate $\eta = \eta_I / \sqrt{D}$, through the last equation of (6).

If the energy source η is turned off, the system—because of its dampening—reaches a state of equilibrium or rest $\mathbf{r}_{eq} = (x_{eq}, 0, 0, 0)^T$. The only possible value for the linear case is $x_{eq} = 0$, while $x_{eq} = \pm\sqrt{6a/|b|}$ are additional equilibrium points if $b < 0$.

Due to the diffusion matrix $\langle \Xi \Xi^T \rangle$ being singular, the approach through the Fokker-Planck equation is not optimal

²These relations tell us how the characteristic displacement, x , of the oscillator induces the electrical tension V and vice versa.

[21]. Instead of working with the probability density function (pdf) $p(\mathbf{r}(t))$ we use the functional pdf $p[\mathbf{r}(t)]$ [21–25]. This is the pdf of the trajectory $\mathbf{r}(t)$ in phase space—linked to Eq. (6)—and can be studied by path integrals. Using the *Martin-Siggia-Rose* auxiliary fields or *response fields* $\tilde{\mathbf{r}} = (\tilde{x}, \tilde{v}, \tilde{V}, \tilde{\eta})^T$ [26], we have

$$p[\mathbf{r}(t)] = \int \mathcal{D}[\tilde{\mathbf{r}}(t)] e^{-\mathcal{S}[\mathbf{r}(t), \tilde{\mathbf{r}}(t)]}, \quad (8)$$

where the stochastic action \mathcal{S} is

$$\mathcal{S}[\mathbf{r}(t), \tilde{\mathbf{r}}(t)] = \int du \{ \tilde{\mathbf{r}}(u)^T [\dot{\mathbf{r}}(u) - \mathbf{f}(\mathbf{r}(u))] - \lambda \tilde{\eta}^2(u) \}. \quad (9)$$

For simplicity we have taken the initial conditions $\mathbf{r}(t_0) = \mathbf{0}$, since we are only interested in the stationary properties of the model. Likewise, as all the time integrals in this work are given between t_0 and t , we omit these integration limits to simplify the notation.

We can write the action as $\mathcal{S} = \mathcal{S}_G + \mathcal{S}_{\text{Int}}$, separating it into two, a Gaussian action \mathcal{S}_G that contains the bilinear part in the fields and \mathcal{S}_{Int} which contains the nonlinear couplings of the system.³ So we have

$$\mathcal{S}_G = \int du du' \tilde{\mathbf{r}}(u)^T G_0^{-1}(u, u') \mathbf{r}(u'), \quad (10)$$

$$\mathcal{S}_{\text{Int}} = \frac{b}{3!} \int du \tilde{v}(u) x^3(u) - \lambda \int du \tilde{\eta}^2(u), \quad (11)$$

where $G_0^{-1}(t, t') = G_0^{-1}(t')\delta(t-t')$ is the inverse matrix operator of the Feynman response propagator $G_0(t, t')$, satisfying Green's relation

$$\int du G_0^{-1}(t, u) G_0(u, t') = \delta(t-t')I, \quad (12)$$

where I is the identity matrix. G_0 is called the free propagator associated with the linear part of the system (6).

III. LINEAR SYSTEM

In this part we address the linear case, i.e., $b = 0$. From $p[\mathbf{r}(t)]$ the moment generating functional, $\mathcal{Z}[\mathbf{J}, \tilde{\mathbf{J}}]$ Eq. (A1) (Appendix A), can be expressed as a series given by Eq. (A5). However, for the linear system the series can be summated to give [25]

$$\mathcal{Z}^0[\mathbf{J}, \tilde{\mathbf{J}}] = \mathcal{Z}_G[0, 0] e^{A[\mathbf{J}, \tilde{\mathbf{J}}]}, \quad (13)$$

with $\mathcal{Z}_G[0, 0]$ given by (A2) and

$$\begin{aligned} A[\mathbf{J}, \tilde{\mathbf{J}}] &= \int du du' \mathbf{J}(u)^T G_0(u, u') \tilde{\mathbf{J}}(u') \\ &+ \lambda \int du du' du'' J_i(u') G_{0i\eta}(u', u) J_j(u'') G_{0j\eta}(u'', u). \end{aligned} \quad (14)$$

From now on we use the Einstein summation convention on the Latin indices ($i, k = x, v, V, \eta$).

³This choice of writing the response functional \mathcal{S} with the noise vertex \mathcal{S}_{Int} is appropriate because Feynman's rules are given from [25] or [27] so that we can use them here systematically. Additionally, Feynman's diagrams are drawn with a single propagator, G_0 .

From Eq. (A1) of Appendix A the moments are

$$\left\langle \prod_{i,j,k,l} r_i(t_k) \tilde{r}_j(t_l) \right\rangle^0 = \frac{1}{\mathcal{Z}_G[0,0]} \prod_{i,j,k,l} \frac{\delta}{\delta J_i(t_k)} \frac{\delta}{\delta \tilde{J}_j(t_l)} \mathcal{Z}^0[\mathbf{J}, \tilde{\mathbf{J}}]_{\mathbf{J}=\tilde{\mathbf{J}}=0}. \quad (15)$$

The superscript 0 indicates that it is for the linear harvester. Note that it is not necessary to calculate $\mathcal{Z}_G[0,0]$ to obtain the moments. The first moments are $\langle r_i(t) \rangle^0 = \langle \tilde{r}_i(t) \rangle^0 = 0$, since we have a single equilibrium point at $\mathbf{r}_{eq} = \mathbf{0}$ and $\langle \eta(t) \rangle = 0$. However, $\eta(t)$ perturbs the system away from the rest state, resulting in nonzero higher-order moments. From Eq. (15) we find

$$\langle r_m(t) \tilde{r}_n(t') \rangle^0 = G_{0mn}(t, t'), \quad (16)$$

$$\langle r_m(t) r_n(t') \rangle^0 = 2\lambda \int du G_{0m\eta}(t, u) G_{0n\eta}(t', u). \quad (17)$$

$$\begin{pmatrix} i[k - (w+i)(w+i\zeta)] & w+i\zeta & -ik & \frac{w+i\zeta}{\lambda-iw} \\ -a(w+i\zeta) & w(\zeta-iw) & -kw & \frac{w(\zeta-iw)}{\lambda-iw} \\ -ia & w & i[a - (w+i)w] & \frac{w}{\lambda-iw} \\ 0 & 0 & 0 & \frac{Q(w)}{\lambda-iw} \end{pmatrix}, \quad (21)$$

where $G_0(w)$ is called the reduced free propagator. Applying the Routh-Hurwitz stability criterion to (6) it is verified that the linear system is stable for all values of the parameters [20,28]. Therefore, the poles of $G_0(w)$ have a negative imaginary part.

Using the so-called Feynman diagrams, the terms in the expansion of the moments can be visually represented. The elements of a diagram are points—called vertices v_{nm} —that represent different times, corresponding to the nonlinear interactions in \mathcal{S}_{Int} , and solid lines that represent the propagators of the matrix G_0 that carries on the signal from one variable to another. Time evolves to the left so that a vertex that is to the right of another one corresponds to a previous time.

Vertices are linked by free propagators⁵

$$G_{0ij}(t, t') \equiv \text{---} \longleftarrow \text{---} \quad (22)$$

A vertex v_{ij} couples j fields coming in from the right with i response fields going out to the left, for example,

$$v_{20} = \lambda \int du \tilde{\eta}^2(u) \equiv \begin{array}{c} \tilde{\eta} \\ \diagdown \quad \diagup \\ \bullet \\ \diagup \quad \diagdown \\ \tilde{\eta} \end{array} \quad (23)$$

For simplicity of notation symbol \sim is not added to the second subscript in propagators.

To obtain the propagator we have to solve (12), where

$$G_0^{-1}(t) = \begin{pmatrix} \frac{d}{dt} & -1 & 0 & 0 \\ a & \frac{d}{dt} + 1 & k & -1 \\ 0 & -1 & \frac{d}{dt} + \zeta & 0 \\ 0 & 0 & 0 & \frac{d}{dt} + \lambda \end{pmatrix}. \quad (18)$$

Using the Fourier transformation⁴ at t and t' we get

$$G_0(w, w') = G_0(w) 2\pi \delta(w + w') = \frac{g(w)}{Q(w)} 2\pi \delta(w + w'), \quad (19)$$

with

$$Q(w) = -w^3 - i(\zeta + 1)w^2 + (k + a + \zeta)w + ia\zeta, \quad (20)$$

and the matrix $g(w)$ is given by

The dashed lines are to visualize the fields going out (or in) the vertex in a particular diagram (in this case two response fields \tilde{r}_η). The vertices imply an integration over time. The sources J_i or \tilde{J}_k at the corresponding time are represented by

$$J_i(t) \quad \bullet \text{---} \longleftarrow \text{---} \quad (24)$$

$$\text{---} \longleftarrow \text{---} \bullet \quad \tilde{J}_k(t) \quad (25)$$

Therefore, $\mathcal{A}[\mathbf{J}, \tilde{\mathbf{J}}]$ in Eq. (14) is represented by

$$\mathcal{A}[\mathbf{J}, \tilde{\mathbf{J}}] = \begin{array}{c} J_i \\ \bullet \longleftarrow \bullet \\ \longleftarrow \bullet \\ \bullet \longleftarrow \bullet \\ J_j \end{array} \begin{array}{c} \longleftarrow \\ \longleftarrow \\ \longleftarrow \end{array} \begin{array}{c} \tilde{J}_j \\ \bullet \\ \bullet \\ \bullet \end{array} + \begin{array}{c} J_i \\ \bullet \longleftarrow \bullet \\ \bullet \longleftarrow \bullet \\ \bullet \longleftarrow \bullet \\ J_j \end{array} \begin{array}{c} \longleftarrow \\ \longleftarrow \\ \longleftarrow \end{array} \begin{array}{c} \tilde{J}_j \\ \bullet \\ \bullet \\ \bullet \end{array} \quad (26)$$

Functional derivatives with respect to J_k or \tilde{J}_l remove the corresponding sources (black dots in diagrams). When, evaluating at $\mathbf{J} = \tilde{\mathbf{J}} = 0$, all diagrams that still possess sources are canceled out. With this in mind, we can represent the (16) and (17) moments by diagrams according to

$$\langle r_i(t) \tilde{r}_j(t') \rangle^0 \equiv \text{---} \longleftarrow \text{---} \quad (27)$$

⁴Defined as $f(w) = \int_{-\infty}^{\infty} dt f(t) e^{iwt}$, on the dimensionless variable t . We can obtain the true frequency results making the variable change $w \rightarrow \omega = \gamma_m w/m$.

⁵In this case $t > t'$.

$$\langle r_i(t)r_j(t') \rangle^0 \equiv \begin{array}{c} r_i \\ \swarrow \\ G_{0i\eta} \\ \searrow \\ G_{0j\eta} \\ \swarrow \\ r_j \end{array} \quad (28)$$

Due to the system being linear and the stochastic force having zero mean, only these diagrams contribute. As a consequence,

$$\Delta\omega = \begin{cases} [a+k-1/2 + \sqrt{2(a+k)^2 - a - k + 1/4}]^{1/2} & \text{if } a+k < 1/2, \\ [a+k-1/2 + \sqrt{a+k-1/4}]^{1/2} & \text{if } 1/2 < a+k \leq 1 + \sqrt{2}/2, \\ [a+k-1/2 + \sqrt{a+k-1/4}]^{1/2} \\ \quad - [a+k-1/2 - \sqrt{a+k-1/4}]^{1/2} & \text{if } a+k > 1 + \sqrt{2}/2. \end{cases} \quad (29)$$

The plot of $\Delta\omega$ vs a is shown in Fig. 1 (dotted line). This bandwidth has a maximum value $\sqrt{1 + \sqrt{2}} \approx 1.55$ for $a+k = 1 + \sqrt{2}/2 \approx 1.7$.

For $\zeta \neq 0$ the bandwidth depends on three independent parameters: ζ , k , and a . Figure 1 (2) shows the bandwidth vs a for fixed k (ζ) and different values of ζ (k), from numerical calculations.

The mean electrical power that dissipated in the load resistor is given by

$$\begin{aligned} P_R^0 &= \frac{\langle V_I^2 \rangle_{st}^0}{R} = \frac{m^2 D k_c^2}{\gamma_m^4 R} \langle V^2 \rangle_{st}^0 \\ &= \frac{m^2 D k_c^2}{\gamma_m^4 R} \lim_{t \rightarrow \infty} \langle V^2(t) \rangle^0, \end{aligned} \quad (30)$$

where the subscript st indicates that the average is done in the steady state. Using (17) and (28) we can express

$$\langle V^2(t) \rangle^0 \equiv \begin{array}{c} V \\ \swarrow \\ G_{0V\eta} \\ \searrow \\ G_{0V\eta} \\ \swarrow \\ V \end{array}, \quad (31)$$

and taking the limit $t \rightarrow \infty$ we arrive at

$$\begin{aligned} \langle V^2 \rangle_{st}^0 &= \lim_{t \rightarrow \infty} 2\lambda \int du G_{0V\eta}^2(t, u) \\ &= 2\lambda \int d\tilde{\omega} |G_{0V\eta}(\omega)|^2 \end{aligned} \quad (32)$$

($\tilde{\omega} = \omega/2\pi$), which results in the expression

$$P_R^0 = \frac{m^2 k_c^2 D}{\gamma_m^4 R} \frac{\Phi \lambda (\zeta + \lambda + 1)}{k\lambda + (\lambda + \zeta)(\lambda^2 + \lambda + a)}, \quad (33)$$

the system can be analytically solved, thus getting closed expressions. Obtaining the moment $\langle \prod_{i=1}^M r_i \rangle$ implies that all the diagrams that can be assembled with M outgoing propagators and none incoming must be considered.

Let us calculate the oscillator bandwidth defined as the frequency range $\Delta\omega$ in which the amplitude of the propagator⁶ $|G_{0Vv}(\omega)|^2$ is greater than half the maximum amplitude. For the case $\zeta = 0$ the calculations are greatly simplified and the following analytical expression can be found:

$$\Phi = \frac{1}{(\zeta + 1)(\zeta + k) + a}. \quad (34)$$

The mean power [20] entering the system is

$$\begin{aligned} P_{in}^0 &= \left\langle \frac{dx_I}{ds} \eta_I \right\rangle_{st}^0 = \frac{D}{\gamma_m} \langle v(t)\eta(t) \rangle_{st}^0 \\ &= \frac{D}{\gamma_m} \lim_{t \rightarrow \infty} \langle v(t)\eta(t) \rangle^0. \end{aligned} \quad (35)$$

Therefore, from (17) and (28) we obtain

$$\langle v(t)\eta(t) \rangle^0 \equiv \begin{array}{c} v \\ \swarrow \\ G_{0v\eta} \\ \searrow \\ G_{0\eta\eta} \\ \swarrow \\ \eta \end{array}, \quad (36)$$

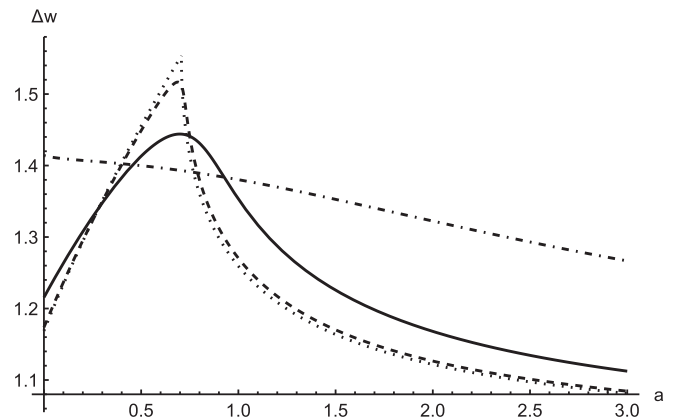


FIG. 1. Bandwidth for the linear oscillator with $k = 1$ and different ζ values: $\zeta = 0$ [Eq. (29), dotted line], $\zeta = 0.01$ (dashed line), $\zeta = 0.1$ (solid line), and $\zeta = 1$ (dash-dotted line).

⁶ $G_{0Vv}(\omega) = V(\omega)/\eta(\omega)$, i.e., the ratio of the voltage and external force, in the Fourier space.

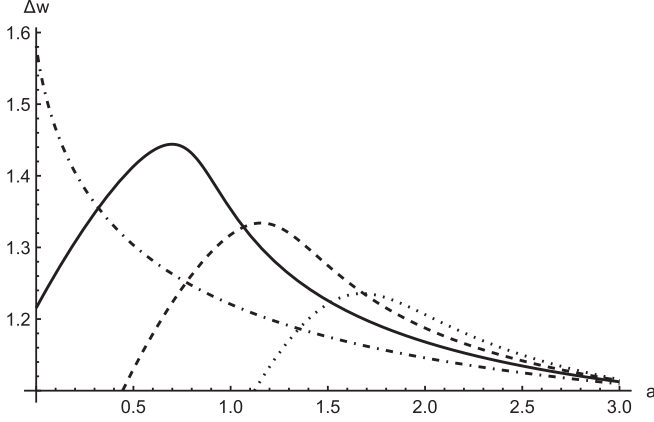


FIG. 2. Bandwidth for the linear oscillator with $\zeta = 0.1$ and different k values: $k = 0$ (dotted line), $k = 0.5$ (dashed line), $k = 1$ (solid line), and $k = 2$ (dash-dotted line).

then

$$\begin{aligned} \langle v\eta \rangle_{st}^0 &= \lim_{t \rightarrow \infty} 2\lambda \int du du G_{0v\eta}(t, u) G_{0\eta\eta}(t, u) \\ &= 2\lambda \int d\tilde{w} G_{0v\eta}(w) G_{0\eta\eta}(-w), \end{aligned} \quad (37)$$

and finally

$$P_{in}^0 = \frac{D}{\gamma_m} \frac{\lambda(\lambda + \zeta)}{k\lambda + (\lambda + \zeta)(\lambda^2 + \lambda + a)}. \quad (38)$$

Therefore, the conversion efficiency of kinetic energy to electrical energy is given by

$$\rho^0 = \frac{P_R^0}{P_{in}^0} = \frac{m}{\gamma_m^2} C k_c^2 \zeta \frac{\zeta + \lambda + 1}{\zeta + \lambda} \Phi. \quad (39)$$

The results of this section agree with those derived previously in [20].

IV. NONLINEAR SYSTEM

In this section we work on system (6) with $b \neq 0$. Then the interaction action (11) generates a new vertex

$$v_{13} = -\frac{b}{3!} \int du \tilde{v}(u) x^3(u) \equiv \tilde{v} \quad (40)$$

An expression like (13) cannot be obtained here and we must work with (A3) (Appendix A) because the new vertex v_{13} produces an infinite amount of terms proportional to powers of b . For example, those that are bilinear in \mathbf{J} and $\tilde{\mathbf{J}}$ will contribute to the propagator, i.e., corrections to the free propagator appear due to the nonlinearity [27,29–33]. However,

rather than calculate all terms up to desired order together with the functional derivatives, we use the utility of the pictorial representation. To obtain the contribution to the free propagator it is necessary to build diagrams with an incoming and an outgoing line (propagators). With both v_{20} and v_{13} the following diagrams can be constructed that contribute to the first order in the perturbative expansion:

$$G_{mn} = \text{---} \leftarrow + \text{---} \leftarrow \text{---} \quad (41)$$

Using the Feynman diagrams representation is useful to obtain the moments without the need to expand the series. A convenient way to deal with the problem is to work in the Fourier space—which converts convolutions into products—and later return to the time domain. In the Fourier representation, the free propagators and nonlinear vertices are written as

$$G_{0mn}(w, w') = G_{0mn}(w) 2\pi \delta(w + w') \quad (42)$$

and

$$\begin{aligned} v_{13} &= -\frac{b}{3!} \int d\tilde{w}_1 d\tilde{w}_2 d\tilde{w}_3 \tilde{v}(w_1) x \\ &\quad \times (w_2) x (w_3) x (-w_1 - w_2 - w_3), \end{aligned}$$

$$v_{20} = \lambda \int d\tilde{w}_1 \tilde{\eta}(w_1) \tilde{\eta}(-w_1).$$

With this, the analytic expression for (41) results in

$$G_{mn}(w) = G_{0mn}(w) - \lambda b G_{0mv}(w) A G_{0xn}(w), \quad (43)$$

where $2\lambda A$ is the correlation of x [to $O(b^0)$], and A , the loop in the diagram, is given by

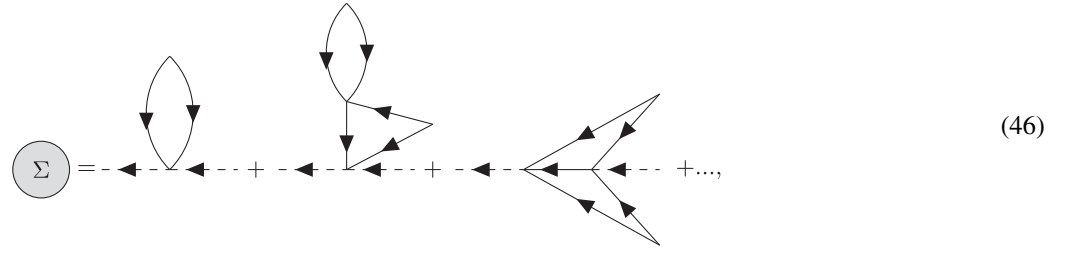
$$\begin{aligned} A &= \int d\tilde{w} |G_{0x\eta}(w)|^2 \\ &= \frac{1}{2a\lambda} \frac{1 + \Phi[a + \zeta(\zeta + 1)][\lambda^2 + \lambda(\zeta + 1)]}{k\lambda + (\zeta + \lambda)(\lambda^2 + \lambda + a)}. \end{aligned} \quad (44)$$

Working analytically with (A3) the first correction appears in $j = 4$ as

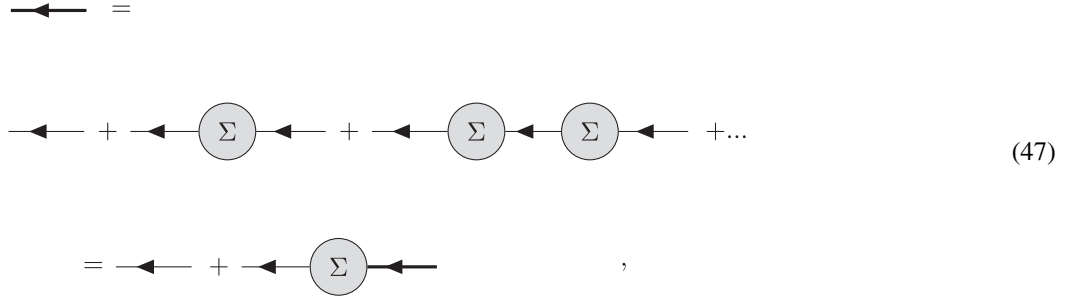
$$\begin{aligned} &-f_s \lambda b \int d\tilde{w}_1 d\tilde{w}_2 d\tilde{w}_3 J_i(-w_1) G_{0iv}(w_1) \\ &\quad \times |G_{0x\eta}(w_2)|^2 G_{0xj}(w_3) \tilde{J}_j(-w_3), \end{aligned} \quad (45)$$

with f_s a symmetry factor that arises from the expansion of the exponential and from the different ways of taking Wick contractions. Then, from variational differentiating the above expression with respect to the sources J_m and \tilde{J}_n , Eq. (43) is recovered.

One way to sort the infinite contributions of b to the free propagator is through the so-called self-energy Σ



which contains the infinite sum of irreducible diagrams that have an outgoing and an incoming field (diagrams 1PI) [27]. Using this object, a diagrammatic equation for the renormalized propagator is obtained



where the thick lines represent renormalized propagators G_{ij} , in contrast to the thin lines, which represent free propagators G_{0ij} . Analytically, the diagrammatic equation (47) results in the Dyson equation [27]

$$G(w) = G_0(w)[1 + \Sigma(w)G_0(w) + \Sigma(w)G_0(w)\Sigma(w)G_0(w) + \dots] = G_0(w)[1 + \Sigma(w)G(w)]. \quad (48)$$

The renormalized matrix propagator in Fourier space is obtained from

$$G^{-1}(w) = G_0^{-1}(w) - \Sigma(w). \quad (49)$$

Due to the shape of the vertex v_{13} , at $O(b)$, we have

$$\Sigma_{ij} = -\lambda b A \delta_{iv} \delta_{jx}. \quad (50)$$

Introducing (50) into (49), the only element that is altered is $G_{0vx}^{-1}(w)$, resulting in

$$G_{vx}^{-1}(w) = G_{0vx}^{-1}(w) + \lambda b A = a + \lambda b A, \quad (51)$$

where we find that a can be renormalized according to

$$a_r = a + \lambda A b, \quad (52)$$

thus obtaining the renormalized propagator to 1 loop

$$G = G_0|_{a=a_r}. \quad (53)$$

Therefore, at $O(b)$, the diagrams for the correlation of two fields are identical to the linear case with thin lines replaced by thick ones, i.e., propagators G in place of free ones G_0 .

Equations (44) and (34) show that $A > 0$. Furthermore, λA does not depend on b and it is bounded (it is only divergent if $a \rightarrow 0$ or if both $\zeta \rightarrow 0$ and $\lambda \rightarrow 0$). Figure 3 show how λA varies on each parameter, leaving the rest fixed.

We can analyze the bandwidth from the linear case by replacing $a \rightarrow a_r$. We see that for both positive and negative b the bandwidth can increase or decrease (with respect to the linear case) according to the graphs 1 and 2. It is worth noting that—unlike the linear case—the response and, therefore, the bandwidth become functions of the characteristic correlation frequency λ due to replacing a by $a_r(\lambda)$ in Eq. (53) and consequently in Eq. (29). This is a consequence of nonlinearity because it couples different modes of vibration.

To calculate the output and input powers we need the correlations $\langle V^2(t) \rangle$ and $\langle v(t)\eta(t) \rangle$. Analogously to the linear

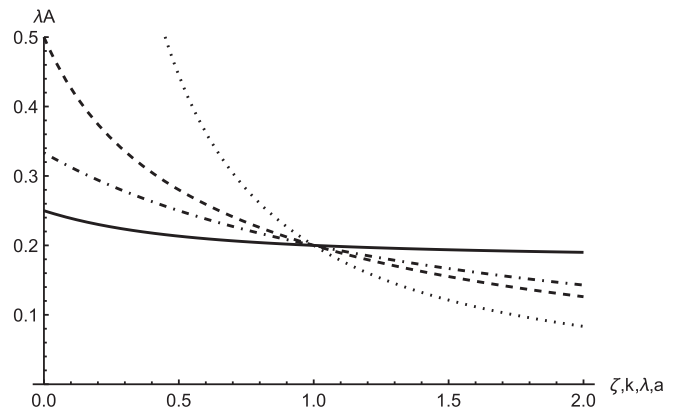


FIG. 3. Factor λA from Eq. (52) vs ζ and $k = \lambda = a = 1$ (solid line), vs k and $\zeta = \lambda = a = 1$ (dot-dashed line), vs λ and $\zeta = k = a = 1$ (dashed line), and vs a and $\zeta = k = \lambda = 1$. All curves intersect at $A\lambda|_{\zeta=k=\lambda=a=1} = 0.2$.

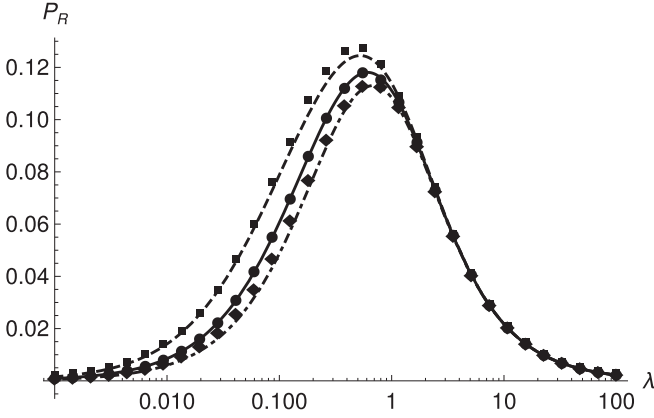


FIG. 4. Mean electrical power harvested on a load resistor R . The lines correspond to Eq. (56) and the points to the numerical results, for $\beta = 0$ (solid with circles), $\beta = -0.1$ (dash with squares), and $\beta = 0.1$ (dot-dash with diamonds). The remaining parameters are $\alpha = 0.5$ and $k_c = k_v = m = \gamma_m = C = R = D = \lambda_l = 1$.

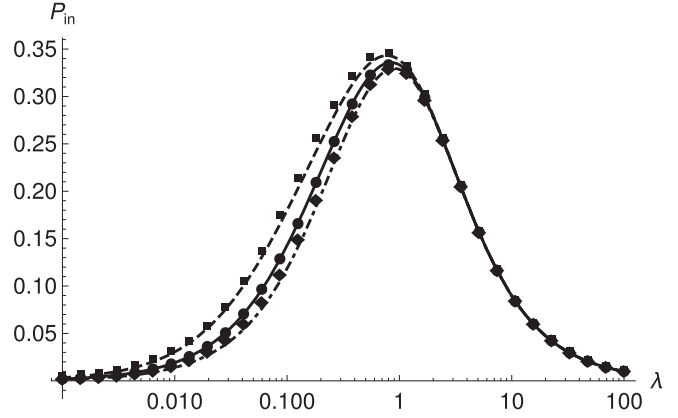


FIG. 5. Mean input power from the forcing η . Same parameters and indicators as in Fig. 4.

case we have

$$\langle V^2(t) \rangle \equiv \begin{array}{c} V \\ \swarrow \quad \searrow \\ G_{V\eta} \quad G_{V\eta} \\ \swarrow \quad \searrow \\ V \end{array} \quad (54)$$

whose analytical expression is

$$\begin{aligned} \langle V^2 \rangle_{st} &= \lim_{t \rightarrow \infty} 2\lambda \int du G_{V\eta}^2(t, u) \\ &= 2\lambda \int d\tilde{w} |G_{V\eta}(w)|^2, \end{aligned} \quad (55)$$

so that the electrical power harvested by the nonlinear system is

$$P_R = P_R^0|_{a=a_r}. \quad (56)$$

In Fig. 4 we plot Eq. (56) together with the numerical integration of the system (6) (using the Heun method) for different values of the parameter b . The good agreement between the simulations and the theoretical result is apparent. Since $A > 0$, from Eq. (52) we see that for $b > 0$ we get $a_r > a$, which reduces the output power, while for $b < 0$ the performance increases. However, such an improvement is bounded due to the stability condition imposed by the Routh-Hurwitz criterion,⁷ namely

$$b > -\frac{a}{\lambda A}. \quad (57)$$

However, it does not mean that the nonlinear system was stable since a negative b produces an inverted quartic potential. In

practice, some kind of stopper must be added to keep the oscillations inside the potential well. Another point of view can be to consider the next term in the restorative potential, i.e., up to the sixth power [$U(x) = \frac{1}{2}ax^2 + \frac{1}{4!}bx^4 + \frac{1}{6!}cx^6$, with $a, c > 0$ and negative or positive b] solving instability problems. This new term produces an analogous first correction to a , namely $a_r = a + b\lambda A + \frac{c}{12}(\lambda A)^2$. Then, if $a + b\lambda A < 0$ one needs to include $\frac{c}{12}(\lambda A)^2$ to fix it. But, if $a + b\lambda A + \frac{c}{12}(\lambda A)^2 < 0$ one only needs to include the next order in the perturbative expansion.

Proceeding in a similar way the input power is obtained by substituting a_r in place of a in the linear harvester expressions, i.e.,

$$P_{in} = P_{in}^0|_{a=a_r}. \quad (58)$$

Figure 5 shows P_{in} , where it can be seen that it has a dependency with b similar to P_R . Therefore, the efficiency ρ for Duffing's nonlinear harvester, shown in Fig. 6, is given by

$$\rho = \rho^0|_{a=a_r} = \frac{m}{\gamma_m^2} C k_c^2 \zeta \frac{\zeta + \lambda + 1}{\zeta + \lambda} \Phi|_{a=a_r}, \quad (59)$$

which only differs from ρ^0 in the expression for Φ .

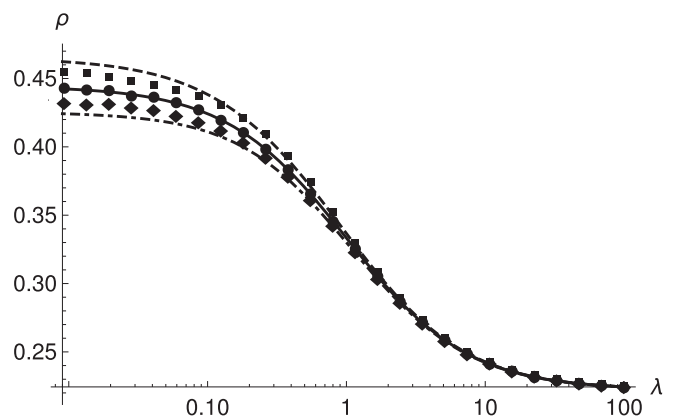


FIG. 6. Mean efficiency ρ . Same parameters and indicators as in Fig. 4.

⁷This criteria is in the effective linear system. It means that a linear harvester with an effective stiffness must satisfy $a_r > 0$.

V. CONCLUSIONS

In this work, the field theory formalism was introduced to the study of stochastic energy harvesters. It was applied to a Duffing harvester driven by an Ornstein-Uhlenbeck noise. Using Feynman diagrams, the internal dynamics of the system can be visualized in a different way.

In the first part the linear case is solved, corroborating the previous results of Mendez *et al.* [20]. Next, the general case is approached analytically by means of a perturbative expansion in b —coefficient of the nonlinear term of the potential—to first order. The main result is a renormalization of the $a \rightarrow a_r$ parameter. This means that a nonlinear harvester behaves—to first order—in the same way as a linear harvester with an effective Hooke parameter $a = a_r$.

It was shown that for $b < 0$ the three performance indicators (harvested power, input power, and efficiency) improve monotonically with $|b|$. However, since b is bounded below by the stability condition of the system, such improvement is limited. We also show that the bandwidth depends nontrivially on b and the characteristic frequency of the noise.

We note that at next order in b new diagrams are found that contribute by introducing a frequency dependency such that $a \rightarrow a(w)$.

As a final comment, this formalism can be extended, through an iterative solution, to the case of non-Gaussian noises knowing $\langle \eta(t) \rangle$ and $\langle \eta(t)\eta(t') \rangle$ [27].

APPENDIX A: GENERATING FUNCTIONAL AND ITS PERTURBATIVE EXPANSION

The moment generating functional is

$$\begin{aligned} \mathcal{Z}[\mathbf{J}, \tilde{\mathbf{J}}] &= \int \mathcal{D}[\mathbf{r}(t)] \mathcal{D}[\tilde{\mathbf{r}}(t)] e^{-S[\mathbf{r}(t), \tilde{\mathbf{r}}(t)]} e^{\int du \mathbf{J}(u)^T \mathbf{r}(u) + \int du \tilde{\mathbf{J}}(u)^T \tilde{\mathbf{r}}(u)}. \end{aligned} \quad (\text{A1})$$

Multiplying and dividing by the free functional

$$\mathcal{Z}_G[0, 0] = \int \mathcal{D}\mathbf{r} \mathcal{D}\tilde{\mathbf{r}} e^{-S_G[\mathbf{r}(t), \tilde{\mathbf{r}}(t)]}, \quad (\text{A2})$$

$$\begin{aligned} \langle \mu^2 \rangle_G &= \left\langle \left(\lambda \int du \tilde{\eta}^2(u) + \int du \mathbf{J}(u)^T \mathbf{r}(u) + \int du \tilde{\mathbf{J}}(u)^T \tilde{\mathbf{r}}(u) \right)^2 \right\rangle_G = 2 \int du du' J_i(u) \langle r_i(u) \tilde{r}_k(u') \rangle_G \tilde{J}_k(u') \\ &= 2 \int du du' J_i(u) G_{0ik}(u, u') \tilde{J}_k(u'). \end{aligned} \quad (\text{A7})$$

All other combinations belonging to $j = 2$ are canceled out.

For $j = 3$ we have

$$\begin{aligned} \langle \mu^3 \rangle_G &= \left\langle \left(\lambda \int du \tilde{\eta}^2(u) + \int du \mathbf{J}(u)^T \mathbf{r}(u) + \int du \tilde{\mathbf{J}}(u)^T \tilde{\mathbf{r}}(u) \right)^3 \right\rangle_G \\ &= 3\lambda \int du du' du'' \langle \tilde{\eta}^2(u) r_i(u') r_k(u'') \rangle_G J_i(u') J_k(u'') \\ &= 3\lambda \int du du' du'' J_i(u') G_{0i\eta}(u', u) J_k(u'') G_{0k\eta}(u'', u). \end{aligned} \quad (\text{A8})$$

The moments $\langle \mu^j \rangle_G$ with $j > 3$ are combinations of these three: $\langle \mu \rangle_G$, $\langle \mu^2 \rangle_G$, and $\langle \mu^3 \rangle_G$.

we get

$$\begin{aligned} \mathcal{Z}[\mathbf{J}, \tilde{\mathbf{J}}] &= \mathcal{Z}_G[0, 0] \langle e^{-S_{\text{Int}}[\mathbf{r}(t), \tilde{\mathbf{r}}(t)] + \int du \mathbf{J}(u)^T \mathbf{r}(u) + \int du \tilde{\mathbf{J}}(u)^T \tilde{\mathbf{r}}(u)} \rangle_G \\ &= \mathcal{Z}_G[0, 0] \left\langle 1 + \sum_{j=1}^{\infty} \frac{\mu^j}{j!} \right\rangle_G, \end{aligned} \quad (\text{A3})$$

with

$$\mu = -S_{\text{Int}} + \int du \mathbf{J}(u)^T \mathbf{r}(u) + \int du \tilde{\mathbf{J}}(u)^T \tilde{\mathbf{r}}(u). \quad (\text{A4})$$

Equation (A3) expresses \mathcal{Z} as a Gaussian average expansion of the nonlinear terms and sources \mathbf{J} and $\tilde{\mathbf{J}}$. Such as $\mathcal{Z}_G \propto \exp \int du du' \mathbf{J}(u)^T G_0(u, u') \tilde{\mathbf{J}}(u')$ has the first null moments $\langle \mathbf{r}(t) \rangle_G = \langle \tilde{\mathbf{r}}(t) \rangle_G = 0$, and it is bilinear in the variables \mathbf{r} and $\tilde{\mathbf{r}}$, Wick's theorem states that only combinations with the same number of fields and response fields survive. Given that $\langle r_i(t) \tilde{r}_j(t') \rangle_G = G_{0ij}(t, t') \propto \theta(t - t')$ (θ is the Heaviside function) we must take into account only the contributions coming from different integrals in the expansion [25].

For the linear case ($b = 0$) one way to obtain the functional \mathcal{Z}^0 is to expand the powers μ^j and then do the Gaussian contractions, resulting in

$$\begin{aligned} \frac{\mathcal{Z}^0[\mathbf{J}, \tilde{\mathbf{J}}]}{\mathcal{Z}_F[0, 0]} &= 1 + \int du du' J_i(u) G_{0ik}(u, u') \tilde{J}_k(u') \\ &\quad + \lambda \int du du' du'' J_i(u') G_{0i\eta}(u', u) J_k(u'') \\ &\quad \times G_{0k\eta}(u'', u) + \dots, \end{aligned} \quad (\text{A5})$$

where the Einstein summation convention over repeated Latin indices, ($i, k = x, v, V, \eta$), has been used. It can be noted that the terms start to get complicated and calculating higher orders becomes laborious very quickly.

We see the first terms of the series (A3) with $b = 0$. For $j = 1$ we have (applying Wick's Theorem)

$$\begin{aligned} \langle \mu \rangle_G &= \left\langle \lambda \int du \tilde{\eta}^2(u) + \int du \mathbf{J}(u)^T \mathbf{r}(u) + \int du \tilde{\mathbf{J}}(u)^T \tilde{\mathbf{r}}(u) \right\rangle_G \\ &= 0. \end{aligned} \quad (\text{A6})$$

For $j = 2$ we have

APPENDIX B: VARIABLE AND PARAMETER TRANSFORMATIONS

In following, we show the table of transformations of variables and parameters made in Sec. II. See Table I for the main variables and parameters used.

TABLE I. Main variables and parameters used. T , L , M , and V in the dimensions columns refers to time, length, mass, and electric potential, respectively. In the last column we can see that the number of parameters is reduced in three after transforming the dynamical equations.

Variable	Dimensions	Dimensionless variable
s	T	$t = \frac{\gamma_m}{m} s$
ω	T^{-1}	$w = \frac{m}{\gamma_m} \omega$
x_I	L	$x = \frac{\gamma_m^2}{m\sqrt{D}} x_I$
V_I	V	$V = \frac{\gamma_m^2}{m\sqrt{D}k_c} V_I$
η_I	MLT^{-2}	$\eta = \frac{1}{\sqrt{D}} \eta_I$
Parameter	Dimensions	Dimensionless parameter
γ_m	MT^{-1}	1
α	MT^{-2}	$a = \frac{m}{\gamma_m} \alpha$
k_c	VM^{-1}	1
k_V	$MLV^{-1}T^{-2}$	$k = \frac{mk_c k_V}{\gamma_m^2}$
$\gamma_e = \frac{1}{RC}$	T^{-1}	$\zeta = \frac{m}{\gamma_m} \gamma_e$
D	$M^2L^2T^{-4}$	1
λ_I	T^{-1}	$\lambda = \frac{m}{\gamma_m} \lambda_I$
β	$ML^{-2}T^{-2}$	$b = \frac{m^3 D}{\gamma_m^6} \beta$

[1] S. Roundy, P. K. Wright, and J. M. Rabaey, *Energy Scavenging for Wireless Sensor Networks with Special Focus on Vibrations* (Springer, Boston, MA, 2004).

[2] F. Shaikh and S. Zeadally, Energy harvesting in wireless sensor networks: A comprehensive review, *Renew. Sust. Energ. Rev.* **55**, 1041 (2016).

[3] C. Covaci and A. Gontean, Piezoelectric energy harvesting solutions: A review, *Sensors* **20**, 3512 (2020).

[4] S. Sojan and R. K. Kulkarni, A comprehensive review of energy harvesting techniques and its potential applications, *Int. J. Comput. Appl.* **139**, 14 (2016).

[5] T. K. Saha, J. N. E. Lucero, J. Ehrich, D. A. Sivak, and J. Bechhoefer, Bayesian information engine that optimally exploits noisy measurements, *Phys. Rev. Lett.* **129**, 130601 (2022).

[6] T. Kaźmierski and S. E. Beeby, *Energy Harvesting Systems: Principles, Modeling and Applications* (Springer, Berlin, 2011).

[7] S. Sudevalayam and P. Kulkarni, Energy harvesting sensor nodes: Survey and implications, *IEEE Commun. Surv. Tutor.* **13**, 443 (2011).

[8] P. Mitcheson, E. Yeatman, G. Rao, A. Holmes, and T. Green, Energy harvesting from human and machine motion for wireless electronic devices, *Proc. IEEE* **96**, 1457 (2008).

[9] S. Beeby and N. M. White, *Energy Harvesting for Autonomous Systems* (Artech House, Norwood, MA, 2010).

[10] S. P. Beeby, M. J. Tudor, and N. M. White, Energy harvesting vibration sources for microsystems applications, *Measur. Sci. Technol.* **17**, R175 (2006).

[11] D. Zhu, M. Tudor, and S. Beeby, Strategies for increasing the operating frequency range of vibration energy harvesters: a review, *Meas. Sci. Technol.* **21**, 022001 (2010).

[12] L. Gammaitoni, H. Vocca, I. Neri, F. Travasso, and F. Orfei, Vibration energy harvesting: Linear and nonlinear oscillator approaches, in *Sustainable Energy Harvesting Technologies - Past, Present and Future*, IntechOpen. Available online: <https://www.intechopen.com/chapters/25373>.

[13] L. Gammaitoni, I. Neri, and H. Vocca, The benefits of noise and nonlinearity: Extracting energy from random vibrations, *Chem. Phys.* **375**, 435 (2010).

[14] Y. Jia, Review of nonlinear vibration energy harvesting: Duffing, bistability, parametric, stochastic and others, *J. Intell. Mater. Syst. Struct.* **31**, 921 (2020).

[15] L. Gammaitoni, I. Neri, and H. Vocca, Nonlinear oscillators for vibration energy harvesting, *Appl. Phys. Lett.* **94**, 164102 (2009).

[16] F. Cottone, H. Vocca, and L. Gammaitoni, Nonlinear energy harvesting, *Phys. Rev. Lett.* **102**, 080601 (2009).

[17] S. D. Nguyen and E. Halvorsen, Nonlinear springs for bandwidth-tolerant vibration energy harvesting, *J. Microelectromech. Syst.* **20**, 1225 (2011).

[18] R. Ramlan, M. Brennan, B. Mace, and I. Kovacic, Potential benefits of a non-linear stiffness in an energy harvesting device, *Nonlinear Dyn.* **59**, 545 (2010).

[19] E. Halvorsen, Energy harvesters driven by broadband random vibrations, *J. Microelectromech. Syst.* **17**, 1061 (2008).

- [20] V. Méndez, D. Campos, and W. Horsthemke, Efficiency of harvesting energy from colored noise by linear oscillators, *Phys. Rev. E* **88**, 022124 (2013).
- [21] H. S. Wio, *Path Integrals for Stochastic Processes* (World Scientific, Singapore, 2013).
- [22] F. Wiegel, *Introduction to Path-Integral Methods in Physics and Polymer Science* (World Scientific, Singapore, 1986).
- [23] H. S. Wio, P. Colet, M. San Miguel, L. Pesquera, and M. A. Rodríguez, Path-integral formulation for stochastic processes driven by colored noise, *Phys. Rev. A* **40**, 7312 (1989).
- [24] M. Chaichian and A. Demichev, *Path Integrals in Physics: Volume I Stochastic Processes and Quantum Mechanics* (CRC Press, Boca Raton, FL, 2018).
- [25] C. C. Chow and M. A. Buice, Path integral methods for stochastic differential equations, *J. Math. Neurosci.* **5**, 8 (2015).
- [26] P. C. Martin, E. Siggia, and H. Rose, Statistical dynamics of classical systems, *Phys. Rev. A* **8**, 423 (1973).
- [27] U. C. Täuber, *Critical Dynamics: A Field Theory Approach to Equilibrium and Non-Equilibrium Scaling Behavior* (Cambridge University Press, Cambridge, UK, 2014).
- [28] F. Golnaraghi and B. C. Kuo, *Automatic Control Systems* (McGraw-Hill Education, New York, 2017).
- [29] J. Binney, N. Dowrick, A. Fisher, and M. Newman, *The Theory of Critical Phenomena: An Introduction to the Renormalization Group* (Clarendon Press, Oxford, 1992).
- [30] J. Cardy, *Scaling and Renormalization in Statistical Physics*, Cambridge Lecture Notes in Physics (Cambridge University Press, Cambridge, UK, 1996).
- [31] N. Goldenfeld, *Lectures on Phase Transitions and the Renormalization Group* (CRC Press, Boca Raton, FL, 2018).
- [32] M. Kardar, *Statistical Physics of Fields* (Cambridge University Press, Cambridge, UK, 2007).
- [33] M. L. Bellac and G. Barton, *Quantum and Statistical Field Theory* (Oxford University Press, Oxford, 1991).